Journal Pre-proof

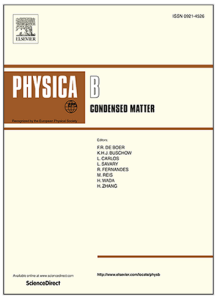

Dielectric tensor of a rectangular arrangement of Ag nanoparticles in anisotropic $LiNbO_3$: Analysis of the negative epsilon conditions

R.M. de la Cruz, C. Kanyinda-Malu, J.E. Muñoz Santiuste

PII: S0921-4526(19)30836-1
DOI: https://doi.org/10.1016/j.physb.2019.411957
Reference: PHYSB 411957

To appear in: *Physica B: Physics of Condensed Matter*

Received date : 2 August 2019
Revised date : 12 December 2019
Accepted date : 16 December 2019

Please cite this article as: R.M. de la Cruz, C. Kanyinda-Malu and J.E. Muñoz Santiuste, Dielectric tensor of a rectangular arrangement of Ag nanoparticles in anisotropic $LiNbO_3$: Analysis of the negative epsilon conditions, *Physica B: Physics of Condensed Matter* (2019), doi: https://doi.org/10.1016/j.physb.2019.411957.

Dielectric tensor of a rectangular arrangement of Ag nanoparticles in anisotropic $LiNbO_3$: analysis of the negative epsilon conditions

R M de la Cruz[a,1,*], C Kanyinda-Malu[b], J E Muñoz Santiuste[c]

[a] *Departamento de Física, Universidad Carlos III de Madrid, EPS. Avda. de la Universidad 30, 28911 Leganés (Madrid), Spain*
[b] *Departamento de Economía Financiera y Contabilidad II, Area de Matemáticas y Estadística, Universidad Rey Juan Carlos, FCJS, Paseo de los Artilleros s/n, 28032 Madrid, Spain*
[c] *Departamento de Física, Universidad Carlos III de Madrid, EPS. Avda. de la Universidad 30, 28911 Leganés (Madrid), Spain*

Abstract

In the present paper we report the optical response of an ordered array of silver (Ag) nanoparticles (NPs) using the uniaxial $LiNbO_3$ as a model case. We investigate the anisotropic effects on the effective dielectric tensor taking into account the charges interaction of particles. The Ag NPs dielectric function is described through a modified Drude model whereas the $LiNbO_3$ dielectric functions are deduced from their experimentally established Sellmeier equations. The effective dielectric tensor components of the ensemble aggregates of Ag NPs and uniaxial $LiNbO_3$ crystal are treated through the extended Maxwell–Garnett approximation. Following the asymmetric behaviour of uniaxial crystals, Ag NPs are sited in the ordinary plane of the crystal, giving rise to different responses in the x, y and z directions of applied electric field. Real and imaginary parts of the effective dielectric tensor components of the aggregate ensemble are investigated in terms of different structural parameters, such as the interparticle spacings, the NPs filling factor and sizes of spherically embedded nanoparticles. We demonstrate that

*Corresponding author
Email addresses: rmc@fis.uc3m.es (R M de la Cruz), clement.kanyindamalu@urjc.es (C Kanyinda-Malu), jems@fis.uc3m.es (J E Muñoz)
[1]Phone: +34 91 624 8733,Fax: +34 91 624 8749

an adequate choice of structural parameters such as NPs sizes, interparticle separation gaps or the filling factor can determine the optical properties of layered Ag–embedded uniaxial crystals such as $LiNbO_3$. We show that the negative epsilon (NE) condition is satisfied from a critical size of Ag NPs when the filling factor and the interparticles distances (a and b) have particular values. This condition defines an interval of energies, called NE range, which clearly depend on values of structural parameters defined in the model. This NE range shows some type of bandwidth anisotropy when it is compared among the x-, y-, z- and xy-components of the effective dielectric tensor. We analyze some anisotropic features such as the bandwidth and shift resonance energies in the real and imaginary parts of the dielectric tensor when structural parameters change.

Keywords:
Array of Ag NPs, Lithium Niobate, Extended Maxwell–Garnett theory, Dielectric properties
PACS: 77.22-d, 78.20.Ci

1. Introduction

The manipulation of light–matter interaction phenomena at the nanoscale by means of plasmonic nanostructures is currently a subject of an intense activity from both fundamental and technological points of view [1, 2, 3]. Noble metal nanostructures exhibit the capability to couple light with the collective oscillations of their conduction–band electrons, known as surface plasmon resonances (SPR), which can result into a strong confinement of the electromagnetic field in the vicinity of the metallic physical boundaries. This can be used to enhance the interactions between far–field light and optical emitters placed in close proximity with the metallic nanostructures [1, 4]. In fact, plasmonic nanostructures can be exploited to improve the performances of existing optical and optoelectronic devices, such as light–emitting systems [4, 5, 6, 7], biosensors [8], solar cells [9, 10], or high–resolution fluorescence microscopes [11]. Additionally, the association of metallic nanostructures with different laser gain media has given rise to successful configurations such as nanolasers or lasing–spasers [12, 13].

Recently, some authors have shown the interest in combining the optical response of metallic nanostructures with the optically active ferroelectric materials. Indeed, Yannopapas and Paspalakis [14] have designed a multilayered

metamaterial consisting of alternating planes of the ferroelectric $LiTaO_3$ and n–type germanium (Ge) in air. This metamaterial has a negative refractive index and, at the same time, the electromagnetic radiation propagates with a group velocity that is of the order of 10^5 slower than the vacuum one. Furthermore, Yraola et al. [15] and Molina et al. [16] have demonstrated that Nd^{3+}–doped periodically poled $LiNbO_3$ shows a spontaneous emission and nonlinear response enhancement by Ag nanoparticles inclusion. Also, these authors claim that this composite could be a plausible metamaterial with a plenty of applications in non–linear optics among others. In addition, Javid et al. [17] have exhaustively investigated the structural, electronic and optical properties of $LiNbO_3$. Wiesendanger and Guntherodt [18] have shown that $LiNbO_3$ exhibits a significant anisotropy in the spectral region below from 7 eV. In the search of negative index metamaterials (NIM's) having both negative ϵ and μ values, specific physical and geometrical conditions play a key–role in controlling the values of permittivity and permeability [19]. For many plasmonic applications, among the metamaterials made-up with nanoscale noble-metals particles, the silver is preferred to gold due to its sharper LSPR resonances and its ability to span the entire visible spectrum. In a previous work, we show that a random three–dimensional (3D) distribution of Ag NPs embedded in $LiNbO_3$ matrix can exhibit negative epsilon (NE) condition in the visible range of electromagnetic spectrum, after a good control of both the Ag-metallic nanoparticles densities and sizes [20].

In the present paper, the effective dielectric tensor of the rectangular array of Ag NPs on $LiNbO_3$ matrix is evaluated by using an extended Maxwell–Garnett (M–G) theory. Such model is appropriate to consider the plausible anisotropy of the system's dielectric tensor in the ordinary and extraordinary directions of the crystal. From the array´s effective dielectric function, we study the compositional and geometrical parameters which could satisfy the negative epsilon condition. In addition, the M–G theory is extensively applied in different types of systems [21, 22, 23].

In fact, we investigate an ordered rectangular array of Ag NPs on $LiNbO_3$ as a model case, because this system is quite similar to the experimentally grown periodical poled $LiNbO_3$ with Ag NPs inclusions. We show that the array of Ag NPs on $LiNbO_3$ matrix can exhibit NE characteristics in the visible range of electromagnetic spectrum, when a good control of the Ag-metallic nanoparticles densities and sizes along with the appropriate interparticle distances in the rectangular array is done. On the other hand, Kinnan et al. [24] investigated the effect of the particle size and interparticle distance in a

disordered two–dimensional arrays of Ag NPs.

The rest of paper is organized as follows. In section 2, an extended M–G model to take into account the anisotropy of the rectangular array of Ag NPs on $LiNbO_3$ matrix is described. The implementation of the model in our system along with a discussion of the results are given in section 3. The main remarks and conclusion of this work will be given in section 4.

2. Modeling optical response of rectangular arrays of nanoparticles

We investigate a rectangular lattice of spherical ordered Ag-nanoparticles as plasmonic inclusions embedded on an uniaxial $LiNbO_3$ crystal. These Ag nanoparticles are located at lattice sites of a two-dimensional (2D) rectangular array and separated by well-defined interparticle distances a and b, along the x and y axes.

The scheme of the investigated system is shown in figure 1, with R representing the NPs radius while a and b describe the interparticle spacings of adjacent particles.

To mimic the experiments of Yraola et al. [15] we assume that in-plane particles are located in the ordinary plane of $LiNbO_3$ crystal. This converts that new scheme as an extension of a square-lattice arrays simulated by Menegotto et al. [25] and Persson et al. [26] in their theoretical models of interacting particles.

As it is well known, the Maxwell–Garnett (M–G) effective medium theory (EMT) can be used to describe the effective dielectric response of an aggregate composite made-up of metallic nanoparticles embedded in a dielectric medium [27]. That macroscopic model represents a good approximation of the interaction between the electromagnetic wave and the nanostructure in the quasi–static regime. When the particles are randomly distributed in a three–dimensional (3D) system, the sum of dipoles contributing to the local field cancels out on average such that the MG–EMT dielectric function can be calculated using the Clausius–Mossotti equation for the polarization of a single particle [25]; i.e.,

$$\epsilon_{eff} = \epsilon_e \left[1 + \frac{3f(\epsilon^{NP} - \epsilon_e)}{(\epsilon^{NP} + 2\epsilon_e) - f(\epsilon^{NP} - \epsilon_e)} \right]. \tag{1}$$

Here ϵ^{NP} and ϵ_e are the dielectric functions of the inclusion particle and embedding medium, and f is the filling factor of particles in $LiNbO_3$ matrix. Then, the above equation represents the dielectric response of the composite

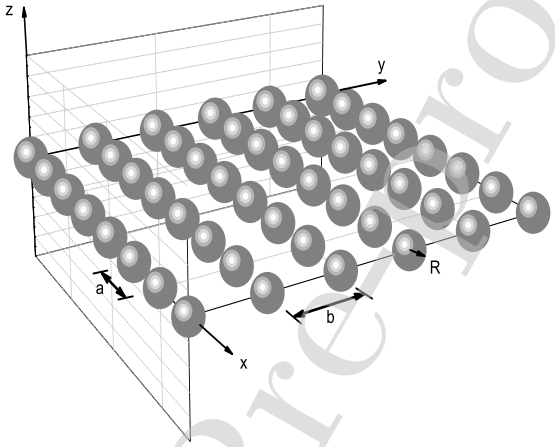

Figure 1: *Scheme of the ordered rectangular array of Ag NPs on a uniaxial $LiNbO_3$ matrix. The parameters a and b represent the interparticle distances along the x and y directions, respectively, where R is the NPs radius.*

for spherical NPs when the depolarization factor is equal to 1/3 [21]. For small f and using the Drude model to describe the dielectric function of the metallic particle, the surface plasmon resonance (SPR) condition is fulfilled at

$$\omega_{SPR} = \frac{\omega_p}{\sqrt{1 + 2\epsilon_e}} \tag{2}$$

where ω_p is the plasma frequency of free electrons in the bulk metal.

In contrast to the 3D random distributions, when metallic nanoparticles are distributed in open systems such as two–dimensional (2D) arrays or linear chains, similar to thin films containing NPs layers, and accounting on interparticles interaction in dipolar approximation; the sum of dipolar electric fields does not cancel out anymore [25]. Accordingly, one may expect dissimilar contributions to the local electric field when the electric field is applied along the x, y or z directions. That dissimilar responses could result in anisotropic responses that can be reflected in different effective dielectric

functions' components for the investigated system.

The anisotropic features in optical responses have been reported elsewhere [28, 29]. At experimental points of view, structural anisotropy such as shape's asymmetry or disorder have been seen to introduce the optical dependence on the orientation of the applied electric field. Also, the anisotropic response can manifest itself through the red-shift or SPR resonances splitting on the spectral positions if the electric field is perpendicular or parallel to particles lines or planes. Another feature commonly ascribed to anisotropic response is the spectral shape asymmetry of the optical bandwidth when we compare the in-plane and out-of plane plasmonic resonances.

Due to the uniaxial symmetry of the crystal, we analyze the diagonal and off–diagonal xy components of the effective dielectric tensor in 2D rectangular system. Such anisotropic dielectric function requires an extended M–G model which accounts for both the plasmon resonance in each particle and the interaction of charges in adjacent particles. That modification will depend on either the nanoparticles are located on a square, an hexagonal or a rectangular array. The geometrical shape of the lattice may introduce new components in the effective dielectric function.

In the following subsection, we describe the diagonal and off-diagonal xy components of the symmetric dielectric tensor when the lattice-NPs are sited in a rectangular array. Most of our calculations will follow and extend the previous works to analyze how such configuration affects or modifies the criteria in simulating negative epsilon conditions.

In our case, ϵ_e is the dielectric function of embedding medium which value has been estimated as the square root of both the ordinary or the extraordinary refractive index (obtained from the Sellmeier expresions of the host medium [30]) depending on the used direction. We use the same notation ϵ_e for both the ordinary and extraordinary directions. In our scheme, see fig. 1, the ordinary directions correspond to the x and y axes, while the extraordinary direction corresponds to z axis. A wavelength of 450 nm is arbitrarily considered to evaluate the Sellmeiller eqs. in this study. For the value of 450 nm (2.76 eV), we have estimated a birefringence ($\Delta n = n_e - n_o$) of 0.11 by considering the data of Javid et al. [17]. For the energy value of 3.5 eV, we have estimated the same birefringence value (0.11) also using the experimental data of the above paper [17]. This result supports the hypothesis that $LiNbO_3$ is anisotropic at the wavelength of $\lambda = 450$ nm.

2.1. Electric fields in a rectangular configuration

Let us define the position vector of each nanoparticle of the 2D-lattice located at the plane $z = 0$ and inside the Lorentz sphere [31]; i.e.,

$$\vec{r} = ia\vec{u}_x + jb\vec{u}_y + 0\vec{u}_z \tag{3}$$

where a and b are the interparticle distances along the x and y axes, respectively; while i and j are integers. We consider that each particle inside this sphere feel the embedding medium as homogeneous. The local field in the system is written as

$$\vec{E}_{loc} = \vec{E}_0 + \Delta\vec{E} + \Delta\vec{E}_i \tag{4}$$

where $\vec{E}_0$ is the applied electric field; $\Delta\vec{E}$ is the electric field due to induced charges in the surface of the sphere and $\Delta\vec{E}_i$ is the electric field due to i^{th} particle inside the Lorentz sphere on the particle located in the sphere center. The electric field $\Delta\vec{E}$ inside an uniformly polarized cell is given by

$$\Delta\vec{E} = \frac{\vec{P}}{3\epsilon_0\epsilon_e}. \tag{5}$$

On the other hand, the polarization of a system of NPs is a function of the NPs density, N, the local field, $\vec{E}_{loc}$ and the polarizability of a nanoparticle, α; then

$$\vec{P} = N\epsilon_0\epsilon_e\alpha\vec{E}_{loc}. \tag{6}$$

Besides, the displacement vector, $\vec{D} = \epsilon_0\epsilon_{eff}\vec{E}_0$ allows to relate the dielectric function of the effective medium with the polarization and the applied field; so the above equation can be written as

$$\vec{P} = \epsilon_0(\epsilon_{eff} - \epsilon_e)\vec{E}_0. \tag{7}$$

If the applied electric field is orthogonal to the NPs 2D lattice, then $\vec{E}_0 = E_0\vec{u}_z$, the polarization of each particle is $\vec{p} = p_z\vec{u}_z$ and the dipolar field is written as

$$\vec{E} = \frac{1}{4\pi\epsilon_0\epsilon_e}\frac{3(\vec{p}.\vec{r})\vec{r} - \vec{p}r^2}{r^5} \tag{8}$$

where the contribution of the dipolar field of all particles inside the Lorentz sphere has only z component; i.e., $\Delta\vec{E}_i$ is

$$\Delta\vec{E}_{iz} = \frac{-p_z\vec{u}_z}{4\pi\epsilon_0\epsilon_e}\sum_{i,j}\frac{1}{(a^2i^2 + b^2j^2)^{3/2}}. \tag{9}$$

Analogously, using the equation (8) with the applied electric field along the x or y directions, the dipolar fields inside the Lorentz sphere are given by

$$\Delta\vec{E}_{ix} = \frac{p_x\vec{u}_x}{4\pi\epsilon_0\epsilon_e}\sum_{i,j}\frac{2a^2i^2 - b^2j^2}{(a^2i^2+b^2j^2)^{5/2}}. \tag{10}$$

and

$$\Delta\vec{E}_{iy} = \frac{p_y\vec{u}_y}{4\pi\epsilon_0\epsilon_e}\sum_{i,j}\frac{2b^2j^2 - a^2i^2}{(a^2i^2+b^2j^2)^{5/2}}. \tag{11}$$

2.2. Modified effective dielectric functions

Then, using eqs. (4), (5), (6), (7), (8) and (9), we deduce the z-component of the effective dielectric tensor

$$\epsilon_{eff,z} = \epsilon_e\left[1 + \frac{3f(\epsilon_z^{NP}-\epsilon_e)}{(\epsilon_z^{NP}+2\epsilon_e) - f(\epsilon_z^{NP}-\epsilon_e) + OR^3(\epsilon_z^{NP}-\epsilon_e)}\right]. \tag{12}$$

Following similar treatment and considering that the applied electric field is $\vec{E}_0 = E_0\vec{u}_x$ or $\vec{E}_0 = E_0\vec{u}_y$, the contribution of the dipolar field of all particles inside the Lorentz sphere has only x or y components. Then, we deduce the x- and y-components of the effective dielectric tensor,i.e.,

$$\epsilon_{eff,x} = \epsilon_e\left[1 + \frac{3f(\epsilon_x^{NP}-\epsilon_e)}{(\epsilon_x^{NP}+2\epsilon_e) - f(\epsilon_x^{NP}-\epsilon_e) - MR^3(\epsilon_x^{NP}-\epsilon_e)}\right], \tag{13}$$

and

$$\epsilon_{eff,y} = \epsilon_e\left[1 + \frac{3f(\epsilon_y^{NP}-\epsilon_e)}{(\epsilon_y^{NP}+2\epsilon_e) - f(\epsilon_y^{NP}-\epsilon_e) - NR^3(\epsilon_y^{NP}-\epsilon_e)}\right], \tag{14}$$

where ϵ_e is evaluated by means of the Sellmeier eqs. [30] which entails different values for the extraordinary (z axis) and ordinary directions (x and y axes) in $LiNbO_3$. In a similar manner, we deduce the off-diagonal xy and yx components of the effective symmetric dielectric tensor; i.e.,

$$\epsilon_{eff,xy} = \epsilon_{eff,yx} = \epsilon_e\left[1 + \frac{3f(\epsilon_{xy}^{NP}-\epsilon_e)}{(\epsilon_{xy}^{NP}+2\epsilon_e) - f(\epsilon_{xy}^{NP}-\epsilon_e) - 3abPR^3(\epsilon_{xy}^{NP}-\epsilon_e)}\right]. \tag{15}$$

On the other hand, the respective terms M, N, O, P and ϵ_{xy}^{NP} are defined in the Appendix.
In the above eqs. (12), (13) and (14), we define the nanoparticle dielectric function along the x, y and z directions as

$$\epsilon_x^{NP}(\omega) = 1 + \frac{f_c\omega_p^2}{(-\omega_{c,x}^2 - \omega^2) - i\Gamma(R)\omega} \tag{16}$$

$$\epsilon_y^{NP}(\omega) = 1 + \frac{f_c\omega_p^2}{(-\omega_{c,y}^2 - \omega^2) - i\Gamma(R)\omega} \tag{17}$$

and

$$\epsilon_z^{NP}(\omega) = 1 + \frac{f_c\omega_p^2}{(2\omega_{c,z}^2 - \omega^2) - i\Gamma(R)\omega} \tag{18}$$

where we have assumed a spring–mass coupling between charges in neighbor particles, in a similar way to that used in ref. [25]. In fact, we have neglected the interband transition of Ag NPs in its dielectric function because we are mainly interested in the SPR along with the charge interactions between NPs. In the above eqs. the size–dependent damping term is $\Gamma(R) = \gamma + Av_F/R$, being γ the bulk damping term, $A = 1$ and v_F the Ag Fermi velocity [32]; f_c accounts for the oscillator strength, where we propose for the coupling frequencies the ansatz

$$\omega_{c,x}^2 \approx B^2\omega_{SPR}^2\left(\frac{R}{a}\right)^3 \tag{19}$$

$$\omega_{c,y}^2 \approx B^2\omega_{SPR}^2\left(\frac{R}{b}\right)^3 \tag{20}$$

and

$$\omega_{c,z}^2 \approx B^2\omega_{SPR}^2\left(\frac{R}{(a+b)/2}\right)^3, \tag{21}$$

respectively. In above eqs. (19), (20) and (21), B is a dimensionless constant. Both constants $B = 3.7$ and $f_c = 0.94$ are taken from reference [25]. Furthermore, the above coupling frequencies are an approach for a rectangular lattice in comparison with a square lattice. We have considered for similarity to the square case that for axis y the interdistance b would be in the definition

of the coupling frequency $\omega_{c,y}$ and for axis z would be the avarage $(a+b)/2$ in the definition of $\omega_{c,z}$.
Finally, using the diagonal and off-diagonal xy components of the symmetric dielectric tensor, we analyze the low loss and negative epsilon conditions $\epsilon''_{eff} \approx 0$ and $\epsilon'_{eff} < 0$ in the investigated arrays to characterize the band-domain of energies for the composite. From mathematical standpoint, imposing low loss or negative epsilon conditions is equivalent to finding structural parameters for which the above criteria are fulfilled. Indeed, to determine how losses and negative epsilon conditions can affect the dielectric response, we discuss the features of resonant energies of ϵ'_{eff} and ϵ''_{eff} for different sets of structural parameters such as f, R, a and b and different directions.

2.3. Extinction cross section

Within the framework of the M–G effective theory, the extinction cross section of the composite is given by [33]

$$\alpha\left(cm^{-1}\right) = \frac{8.88 \times 10^{7}}{\lambda\,(nm)} \sqrt{-\epsilon'_{eff} + \sqrt{(\epsilon'_{eff})^2 + (\epsilon''_{eff})^2}} \tag{22}$$

where λ, the wavelength of the incident light, is given in nanometers, while ϵ'_{eff} and ϵ''_{eff} represent the real and imaginary parts of of the effective symmetric dielectric tensor of the system. We analyze the diagonal and off–diagonal components of this tensor. As it is well known, the extinction cross section is the sum of the absorption and scattering cross sections, being the absorption the greatest contribution to this sum for low–dimensional systems [34], such as observed in our composite.

3. Results and discussion

The simulated plasmonic NPs inclusions and its structural parameters have been schematically described in figure 1. It consists of Ag NPs ordered on a rectangular array and deposited on the uniaxial $LiNbO_3$ crystal. This modeled structure is discussed under an extended Maxwell–Garnett theory, where the interparticles interactions are taken into account. Due to dissimilar responses at applied electric fields along the x, y or z directions, we have different diagonal components of the effective dielectric tensor. In fact, we investigate the diagonal and the off–diagonal xy components of the symmetric dielectric tensor. For our simulations, we choose $2R < a$; i.e., no contacting

nanoparticles and $b = 2a$ for the rectangular arrangement. We evaluate the filling factor as $f = \frac{4\pi R^3/3}{abc}$, where the thickness c is 0.5 μm. So, a change of the NP radius or the gap distances a or b entail a different filling factor. Also, to clarify the presentation of our results, we divide our discussion in different subsections, each one accounting on the effect of selected structural and compositional parameters that determine the dielectric features and the extinction cross section.

3.1. Effects of NPs radius on the dielectric tensor components

Figures 2 and 3 depict the real and imaginary parts of $\epsilon_{eff,x}$, $\epsilon_{eff,y}$ and $\epsilon_{eff,z}$ for a rectangular array of Ag NPs with radii ranging between 10 nm and 100 nm. These values are smaller than the wavelength in the range investigated, validating the use of the quasi–static approximation. Throughout this study, we use following geometrical parameters: $R/a = 0.25$, $R/b = 0.125$ for all investigated cases and f ranging between 0.0026 and 0.026. These values of f are typical within the framework of M–G theory [22]. As shown in figures 2 and 3, we observe several effects of anisotropic characteristics of our system on ϵ'_{eff} and ϵ''_{eff}. Those effects are reflected through the profiles of ϵ'_{eff} and ϵ''_{eff} with distinct resonance energies in the three directions. For a fixed R value, the different resonance energies along the x, y and z directions can be ascribed to the different coupling frequencies along the three directions in the assumed framework of spring–mass coupling between charges in neighbor particles [see eqs. 19 – 21]. As R decreases, for the x direction (i.e., when interparticle distance is a), the resonant peaks in the real part of ϵ_{eff} appear between 2.17 eV and 2.21 eV; while for the y direction (i.e., with the interparticle distance equal to b), the resonant peaks appear between 2.43 eV and 2.47 eV. For the perpendicular direction to the ordinary plane (i.e., z direction) the resonant peaks appear between 2.73 eV and 2.81 eV. Therefore, in all directions the resonances are red-shifted for increasing radii. The bandwidth of this red–shift is around 40–80 meV along the x-, y- and z-directions, showing consequently, some type of anisotropy. Furthermore, this red–shift is analogous to that observed in the optical properties of other low–dimensional systems [35].

For the real part of the effective dielectric tensor components, the negative epsilon (NE) conditions; i.e., $\epsilon'_{eff,x} < 0$, $\epsilon'_{eff,y} < 0$ or $\epsilon'_{eff,z} < 0$ are reached at critical value for radii as large as 80 nm for the three components.

This 2D system presents three specific windows where the positive and negative $\epsilon'_{eff,x}$, $\epsilon'_{eff,y}$ and $\epsilon'_{eff,z}$ may coexist (see figure 2). In fact, Podoloskiy

and Narimanov [36] have demonstrated that for an uniaxial dielectric constant, the negative index material is feasible, when $\epsilon'_{eff,z} < 0$ and $\epsilon'_{eff,||} > 0$ even if the material which is placed in a waveguide shows no magnetic response ($\mu = 1$). However from our findings, we observe that both $\epsilon'_{eff,z} < 0$ and $\epsilon'_{eff,x} > 0$, $\epsilon'_{eff,y} > 0$ or $\epsilon'_{eff,z} > 0$ and $\epsilon'_{eff,x} < 0$, $\epsilon'_{eff,y} < 0$ may coexist at different wavelengths (see fig.2). Some authors have reported that hyberbolic metamaterials can present opposite signs in $\epsilon'_{eff,z} > 0$ and $\epsilon'_{eff,||} < 0$ [38], giving rise to type-I or type-II hyperbolic metamaterials. So, depending on the region under investigation, ordered arrays of Ag NPs grown on an uniaxial crystal such as $LiNbO_3$ can behave either as a type-I or type-II hyberbolic metamaterial.

On the other hand, the NE range (energy interval where NE condition is observed) is approximately between 2.18 eV and 2.31 eV for $\epsilon'_{eff,x}$, between 2.45 eV and 2.57 eV for $\epsilon'_{eff,y}$ and between 2.74 eV and 3.0 eV for $\epsilon'_{eff,z}$ for R = 100 nm (see Fig. 2). Then, the NE range is 130 meV for the x direction, 120 meV for the y direction and 260 meV for the z direction; consequently this feature shows some type of bandwidth anisotropy. For smaller radii, the NE range is narrower in all investigated directions (see Fig.2).

For the imaginary part (see Fig. 3), as R decreases the resonance of $\epsilon''_{eff,x}$ is centered between 2.17 eV to 2.21 eV, while that of $\epsilon''_{eff,y}$ is located between 2.44 eV to 2.47 eV and finally the resonance of $\epsilon''_{eff,z}$ is centered between 2.73 eV and 2.81 eV. In fact, for the three investigated directions, the resonances are red–shifted for increasing radii. The bandwidth of this red–shift is around 30–80 meV for the three directions, showing some anisotropic feature. Also, for the resonant peaks, their FWHM become more and more narrower with increasing radii, while the energy range bandwidth characterized by $\epsilon''_{eff} \approx 0$ becomes wider in the same range.

Figure 4 shows the real and imaginary parts of the off–diagonal components $\epsilon_{eff,xy} = \epsilon_{eff,yx}$ with radii ranging between 10 nm and 100 nm and f ranging between 0.0026 and 0.026. We choose the same values than those investigated for the diagonal components in order to compare both of them. For a fixed R value, the resonant energy of the off–diagonal components is around 1.56 eV, which is smaller than the resonance energies of the diagonal components. This trend show some anisotropic feature due to the assumed framework of spring–mass coupling in neighbor particles [see eqs. 19 – 21 and appendix]. As R decreases, the resonant peaks in the real and imaginary parts of $\epsilon_{eff,xy} = \epsilon_{eff,yx}$ appear between 1.55 eV and 1.58 eV. This

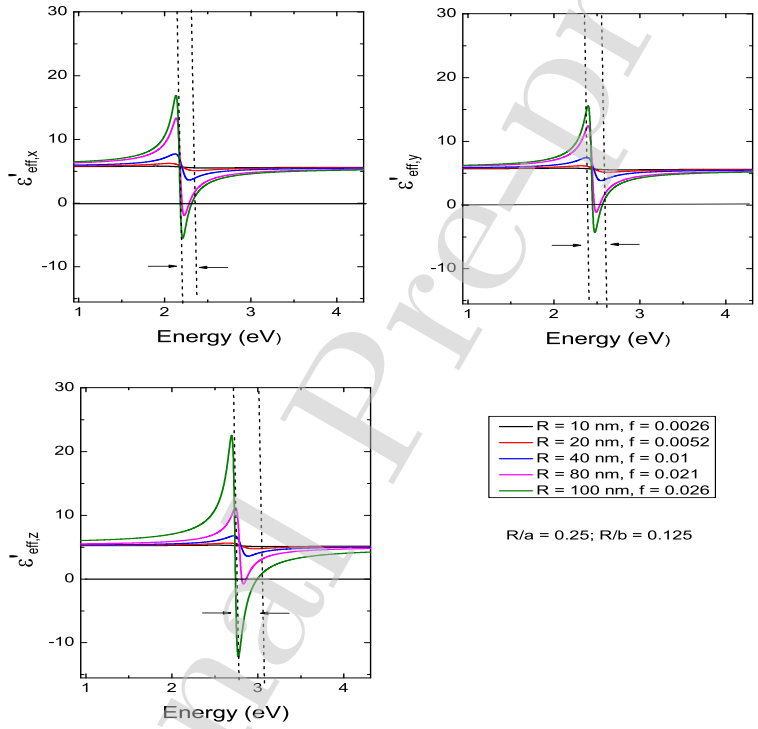

Figure 2: *Real parts of $\epsilon_{eff,x}$, $\epsilon_{eff,y}$ and $\epsilon_{eff,z}$ of the 2D array for different radii and filling factor. The zero-reference line mark out the NE range and the regions between arrows indicate the flip–flop sign.*

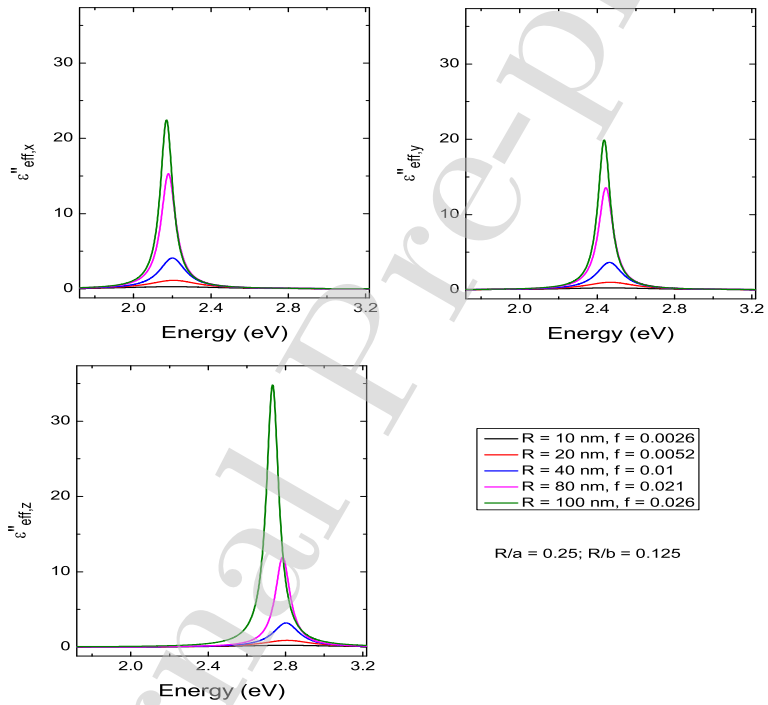

Figure 3: *Imaginary parts of $\epsilon_{eff,x}$, $\epsilon_{eff,y}$ and $\epsilon_{eff,z}$ of the 2D array for different radii and filling factor.*

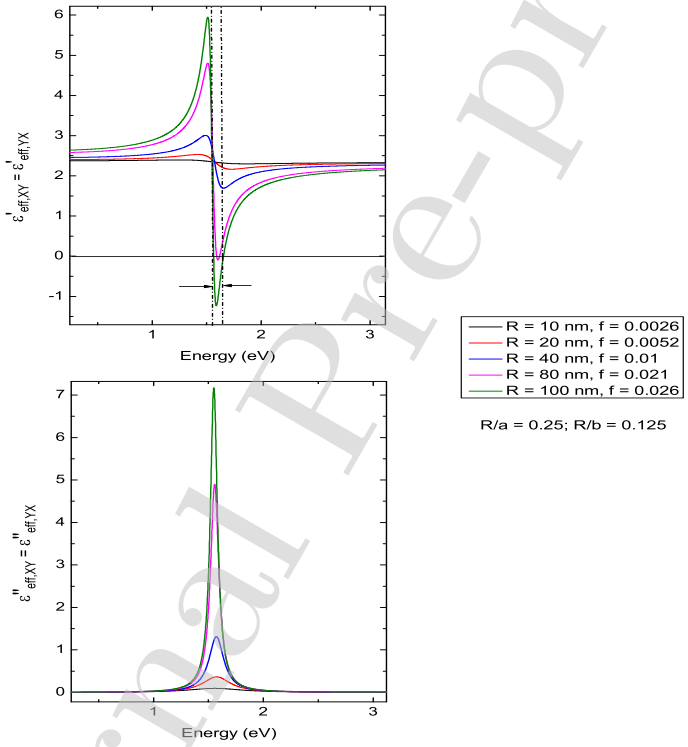

Figure 4: *Real and imaginary parts of $\epsilon_{eff,xy} = \epsilon_{eff,yx}$ of the 2D array for different radii and filling factor. The zero-reference line mark out the NE range.*

red–shift for increasing radii is similar to those obtained in the diagonal components. The trend of red–shift for resonance energies when the radii increase is analogous to that reported in other low–dimensional systems [35]. The NE condition; i.e., $\epsilon'_{eff,xy} < 0$ is reached at the same critical value of 80 nm as for diagonal components, while the NE range at $R = 100$ nm is 90 meV, which is smaller than those obtained in the diagonal components. For the imaginary part of $\epsilon_{eff,xy} = \epsilon_{eff,yx}$, the FWHM of the resonant peaks become more and more narrower with increasing radii, trend which is similar to the FWHM of the diagonal components.

Although we fix the value $\lambda = 450$ nm to evaluate the dielectric constant of $LiNbO_3$, we have evaluated it for other wavelengths. As an example, for $\lambda = 532$ nm (2.33 eV), which entails a smaller refractive index, we obtain that the resonance peaks are blue–shifted respect to our case of $\lambda = 450$ nm; while for $\lambda = 350$ nm (3.54 eV), which entails a higher refractive index, the resonance peaks are red–shifted. This is the expected trend, because for an embedding smaller dielectric constant the resonant peaks are blue–shifted, while for greater values the peaks are red–shifted [37].

3.2. Effects of the interparticle distances on the dielectric tensor components

We show in figures 5 and 6 the real and imaginary parts of $\epsilon_{eff,x}$, $\epsilon_{eff,y}$ and $\epsilon_{eff,z}$ for Ag NPs rectangular arrays with $R = 100$ nm and f ranging between 0.026 and 0.012. In this simulation, the interparticle distance a ranges between 400 nm to 600 nm while the gap distance b lies between 800 nm and 1200 nm. The anisotropy effects on $\epsilon_{eff,x}$, $\epsilon_{eff,y}$ and $\epsilon_{eff,z}$ are clearly noticeable. For fixed a and b values, the different resonance energies along the x, y and z directions can be interpreted in terms of the different coupling frequencies along the three directions as we have discussed in the above subsection. As a and b increase, the resonant peaks in the real part of ϵ_{eff} appear between 2.13 eV and 2.47 eV for the x direction; it lie between 2.40 eV and 2.60 eV for y direction and it ranges between 2.66 eV and 2.78 eV for perpendicular direction. Then, the bandwidth due to the interdistances change is 340 meV in the x direction, 200 meV in the y direction and 120 meV in the z direction; consequently we can infer some type of bandwidth anisotropy. Indeed, the spectral resonant bandwidths together with the peaks position separation are seen to be largely affected by the lateral arrangement of nanoparticles along the x-direction than in y and z ones. To confirm this behaviour (not shown here), we interchange the particles arrangement such that the extraordinary direction of $LiNbO_3$ coincides with x-direction

while y and z directions are in ordinary directions of $LiNbO_3$. We also observe that peaks separations and bandwidths along the x-direction are still more resolved that they are in the y and z directions. That confirms that the spectral anisotropy reported in our simulations are not related with the environment dielectric medium.

On the other hand, the resonance energies are blue–shifted for the x and y directions, while for the z direction the resonance energies are red-shift when the interdistances a and b increase. As the resonance energies shift is more noticeable for $\epsilon_{eff,x}$ than for the other directions, we can explain this feature as follows. The NPs interdistance a is smaller than b and the interaction between neighbor nanoparticles is stronger; consequently, the width shift could be greater for the x direction.

Looking at the fig. 5, we observe that for $\epsilon'_{eff,x}$, $\epsilon'_{eff,y}$ and $\epsilon'_{eff,z}$ the NE condition is fulfilled for the values R/a between 0.25 and 0.2 and the values of R/b between 0.125 and 0.1. Then, to get NE condition it is necessary a critical value of the filling factor f or that the ratios R/a and R/b have particular values. For $\epsilon'_{eff,x}$, $\epsilon'_{eff,y}$ and $\epsilon'_{eff,z}$, the NE range is narrower for increasing distances a and b. In addition, the NE bandwidth is blue–shifted for $\epsilon'_{eff,x}$ and $\epsilon'_{eff,y}$ while for $\epsilon'_{eff,z}$ the NE range is red–shifted. Then, this feature is similar to that obtained for the energy resonances.

As we have previously discussed in section 3.1, we obtain three specific windows where the positive and negative $\epsilon'_{eff,x}$, $\epsilon'_{eff,y}$ and $\epsilon'_{eff,z}$ may coexist (see figure 5). Therefore, depending on the region under investigation and the a and b values, ordered arrays of Ag NPs grown on an uniaxial crystal such as $LiNbO_3$ can behave either as a type-I or type-II hyberbolic metamaterial.

For the imaginary part (see Fig. 6), the resonance peak of $\epsilon''_{eff,x}$ is centered between 2.17 eV and 2.42 eV for increasing interparticle distances, while the resonance of $\epsilon''_{eff,y}$ is observed between 2.43 eV and 2.48 eV and finally the resonance for $\epsilon''_{eff,z}$ lie between 2.66 eV and 2.73 eV. The bandwidth is 250 meV for the x direction, 50 meV for the y direction and 70 meV for z direction. We claim that there is some type of bandwidth anisotropy by investigating the interdistances change. Then, the resonance energies are blue–shifted for the x and y directions, while for the z direction the resonance energies are red-shift when the interdistances a and b increase. This feature is similar to that obtained for the real part. Again, we have that the resonance energies blue–shift is more noticeable for the imaginary part of $\epsilon_{eff,x}$ than for the other directions. It can be explained as the same origin that previously discussed for the real part of the effective dielectric function. On the other

hand, for the three peaks, their FWHM are mainly independent of a or b distances. The range where the low loss condition is fulfilled describes a wide bandwidth.

Although it is not shown here, we have also investigated the effects of the interparticle distances on the off–diagonal components $\epsilon_{eff,xy} = \epsilon_{eff,yx}$. For the real and imaginary parts of the off–diagonal components, the resonance energies are blue–shifted as the interparticle distances a and b increase. For example, when $a = 400\ nm$ and $b = 800\ nm$ ($f = 0.026$, $R = 100\ nm$), the resonance peak is around $1.55\ eV$, when $a = 500\ nm$ and $b = 1000\ nm$ ($f = 0.017$, $R = 100\ nm$), the resonance is peaked around $1.70\ eV$ and finally when $a = 600\ nm$ and $b = 1200\ nm$ ($f = 0.012$, $R = 100\ nm$) the resonance peak is around $1.76\ eV$. This blue–shift is also obtained in the x- and y-diagonal components as it was previously discussed. On the other hand, the NE condition is only fulfilled for $R/a = 0.25$ and $R/b = 0.125$. Then, to get NE condition it is necessary a critical value of filling factor f [20]. This characteristic is analogous to that observed in the diagonal components of the effective symmetric dielectric tensor.

3.3. Effects of structural parameters on the extinction

Firstly, we analyze the extinction dependence on the electric field polarization for a rectangular array of Ag NPs with $R = 100\ nm$ and $f = 0.026$, values for which the NE condition is fulfilled. We define extinction as the extinction cross section multiplied by the NP size as in reference [20]. Figure 7 shows the composite extinction when the applied electric fields are in the x-, y- and z-axes. The resonances are peaked at $2.19\ eV$ (axis x), $2.45\ eV$ (axis y) and $2.75\ eV$ (axis z); i.e., at the same energies that the resonances of $\epsilon_{eff,x}$, $\epsilon_{eff,y}$, $\epsilon_{eff,z}$ for the same R and f values, as it could be expected. On the other hand, althougth it is not shown here, the extinction intensity decreases a factor around 500 when $R = 10\ nm$ and $f = 0.0026$, being the energy resonances slightly blue–shifted respect to higher values of R and f. This behavior with the radius and filling factor is also reported in a 3D distribution of Ag NPs embedded in $LiNbO_3$ [20]. As an example, we show in figure 8 the extinction for the z direction with $R = 100\ nm$, f ranging between 0.026 and 0.012, the interparticle distance a ranges between $400\ nm$ and $600\ nm$, while the gap distance b lies between $800\ nm$ and $1200\ nm$. The resonance energies are peaked around $2.79\ eV$ and $2.68\ eV$, showing a red–shift as a and b increase. This dependence is similar to that discussed for $\epsilon_{eff,z}$ on the interparticle distances. Finally, as the extinction behavior is

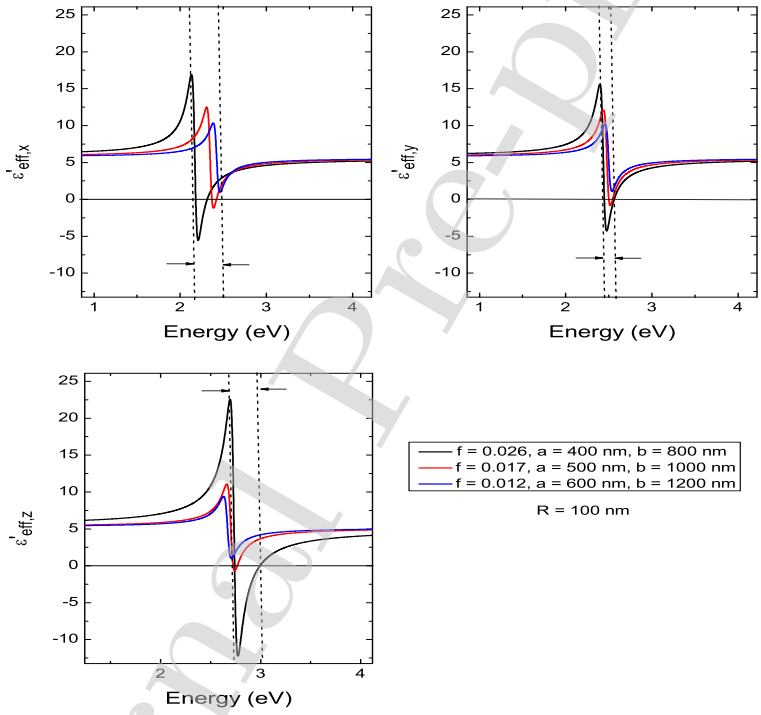

Figure 5: *Real parts of $\epsilon_{eff,x}$, $\epsilon_{eff,y}$ and $\epsilon_{eff,z}$ of the 2D array for different interparticle distances and filling factor. The zero-reference line describes the level under which the NE condition is satisfied and the regions between arrows indicate the flip–flop sign.*

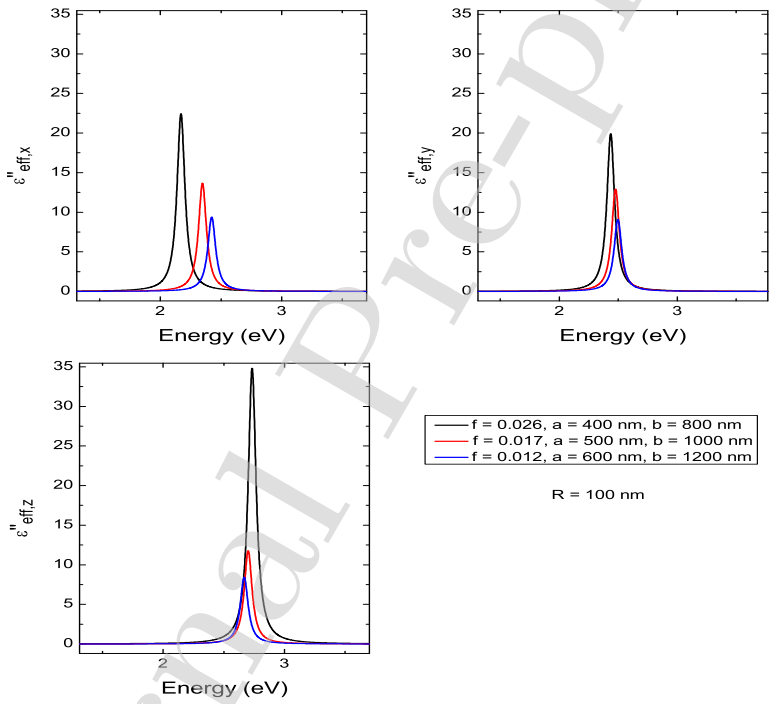

Figure 6: *Imaginary parts of $\epsilon_{eff,x}$, $\epsilon_{eff,y}$ and $\epsilon_{eff,z}$ of the 2D array for different inter-particle distances and filling factor.*

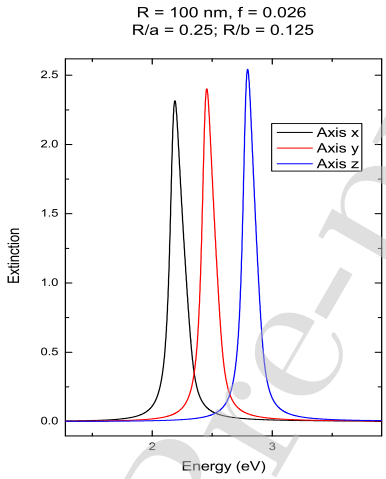

Figure 7: *Extinction dependence on the electric field polarization for a rectangular array of Ag NPs.*

similar to that obtained in the imaginary parts of the symmetric dielectric tensor components, we can conclude that the extinction in the investigated system is mainly due to the absorption process.

4. Conclusions

We have evaluated the diagonal and the off–diagonal components of the effective symmetric dielectric tensor of an ordered rectangular array of Ag NPs on $LiNbO_3$ matrix. Using an extended Maxwell–Garnett effective theory and taking into account the dipolar interaction of neighboring particles, three specific cases of polarized electric field were considered to account on the anisotropic effect on the dielectric response. To describe the Ag NPs and $LiNbO_3$ dielectric functions, we used, respectively, a modified Drude model and the Sellmeier equations. The x- and y-components of the effective dielectric tensor are associated with the "ordinary plane" of $LiNbO_3$ while the

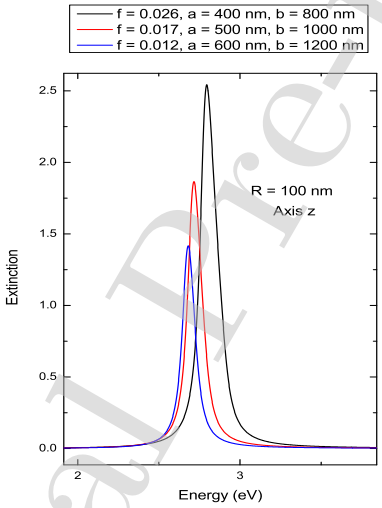

Figure 8: *Extinction for the z axis in a rectangular array of Ag NPs with different filling factors and interdistances a and b.*

z-component is coupled to extraordinary dielectric constant of $LiNbO_3$.

To account of the role of structural parameters, we investigated the effects of NPs radius, rectangular array interparticles distances and filling factor on the dielectric response in the ordinary and extraordinary directions. We showed that the negative epsilon condition is satisfied from a critical size of Ag NPs when the filling factor and the interparticles distances (a and b) have particular values. This condition defines an interval of energies, called NE range, which clearly depend on values of structural parameters defined in the model. This NE range shows some type of bandwidth anisotropy when it is compared among the x-, y-, z- and xy-components. Indeed, we have analyzed some anisotropic features such as the bandwidth and shift resonance energies in the real and imaginary parts of the effective symmetric dielectric tensor when structural parameters change. Finally, we have evaluated the extinction when the applied electric fields are in the x-, y- and z-axes for different R, a, b and f values. We have obtained that varying structural parameters of 2D arrays of Ag NPs, the plasmon resonance can be tuned across the near-UV and visible spectral range, such as it is experimentally observed.

Acknowledgements

This work is partially supported by Spanish MICINN under grant RTI 2018-101020-B-I00 and TECHNOFUSION III CM–S2018IEMAT–4437.

Appendix

The terms M, N, O and P in eqs. (12), (13), (14) and (15) are written as

$$M = \sum_{i,j} \frac{2i^2a^2 - j^2b^2}{(a^2i^2 + b^2j^2)^{5/2}} \tag{A.1}$$

$$N = \sum_{i,j} \frac{2j^2b^2 - i^2a^2}{(a^2i^2 + b^2j^2)^{5/2}} \tag{A.2}$$

$$O = \sum_{i,j} \frac{1}{(a^2i^2 + b^2j^2)^{3/2}}. \tag{A.3}$$

and

$$P = \sum_{i,j} \frac{ij}{(a^2i^2 + b^2j^2)^{5/2}}. \tag{A.4}$$

The above expressions come from the development of the dipolar electric field of all studied particles inside the Lorentz sphere for different polarizations of the applied electric field. The numerical value of M, N, O and P has been evaluated using the Mathematica package. On the other hand, the NP dielectric function $\epsilon_{xy}^{NP} = \epsilon_{yx}^{NP}$ is defined as

$$\frac{\epsilon_x^{NP}\epsilon_y^{NP}}{\epsilon_x^{NP} + \epsilon_y^{NP}} \tag{A.5}$$

which corresponds to the inverse law of dielectric functions [40].

References

[1] L. Novotny and N. van Hulst, Nat. Photonics **5** (2011) 83.

[2] D.K. Gramotnev and S.I. Bozhevolnyi, Nat. Photonics **4** (2010) 83.

[3] J. Liu, H. He, D. Xiao, S. Yin, W. Ji, S. Jiang, D. Luo, B. Wang and Y. Liu, Materials **11** (2018) 1833.

[4] M.L. Debasu, D. Ananias, I. Pastoriza–Santos, L.M. Liz–Marzan, J. Rocha and L.D. Carlos, Adv Mater. **25** (2013) 4868.

[5] D. Elvira, R. Braive, G. Beaudoin, I. Sagnes, J.-P. Hugonin, I. Abram, I. Robert-Philip, P. Lalanne and A. Beveratos, Appl. Phys. Lett.**103** (2013) 061113.

[6] W. Zhou, M. Dridi, J.Y. Suh, C.H. Kim, D.T. Co, M.R. Wasielewski, G.C. Schatz and T.W. Odom, Nat. Nanotechnol.**8** (2013) 506.

[7] G. Lozano, D.J. Lowers, S.R. Rodríguez, S. Murai, O.T. Jansen, M.A. Verschuuren and J.G. Rivas, Light: Sci. Appl. **2** (2013) e66.

[8] E. Hutter and J.H. Fendler, Adv. Mater. **16** (2004) 1685.

[9] H.A. Atwater and A. Polman, Nat. Mat. **9** (2010) 205.

[10] K. Nakayama, K. Tanabe and H.A. Atwater, Appl. Phys. Lett. **93** (2008) 121904.

[11] S.A. Maier, P.G. Kik, H.A. Atwater, S. Meltzer, E. Harel, B.E. Koel and A.A.G. Requicha, Nat. Mater. **2** (2003) 229.

[12] M.A. Noginov, G. Zhu, A.M. Belgrave, R. Bakker, V.M. Shalaev, E.E. Narimanov, S. Stout, E. Herz, T. Suteewong and U. Wiesner, Nature **460** (2009) 1110.

[13] O. Hess, J.B. Pendry, S.A. Maier, R.F. Oulton, J.M. Hamm and K.L. Tsakmakidis, Nat. Mater. **11** (2012) 573.

[14] V. Yannopapas and E. Paspalakis, J. Opt. **12** (2010) 104017.

[15] E. Yraola, P. Molina, J.L. Plaza, M.O. Ramírez and L.E. Bausá, Adv. Mater., **25** (2012) 910.

[16] P. Molina, E. Yraola, M.O. Ramírez, J.L. Plaza, C. Heras and L.E. Bausá, Nano Lett. **13** (2013) 4931.

[17] M.A. Javid, Z.U. Khan, Z. Mehmood, A. Nabi, F. Hussain, M. Imran, M. Nadeem and N. Anjum, Int. J. of Modern Phys. B **32** (2018) 1850168.

[18] E. Wiesendanger and G. Guntherodt, Sol. Stat. Commun. **14** (1974) 303.

[19] A.D. Boardman, V.V. Grimalsky, Y.S. Kivshar, S.V. Koshevaya, M. Lapine, N.M. Litchinitser, V.N. Malnev, M. Noginov, Y.G. Rapoport and V.M. Shalaev, Laser Photon. Rev. **5** (2011) 287.

[20] R.M. de la Cruz, C. Kanyinda–Malu and J.E. Muñoz Santiuste, Mater. Res. Express **4** (2017) 025023.

[21] V.A. Markel, J. Opt. Soc. America A **33** (2016) 1244.

[22] G.A. Niklasson, C.G. Granqvist and O. Hunderi, Appl. Optics **20** (1981) 26.

[23] M. Piralaee, V. Siahpoush and A. Asgari, *Proc. of 6th Int. Conf. on Nanostructures, 7-10 March 2016, Kish Island, Iran.*

[24] M.K. Kinnan and G. Chumanov, J. Phys. Chem. C **114** (2010) 7496.

[25] T. Menegotto and F. Horowitz, Appl. Optics **53** (2014) 2853.

[26] B.N.J. Persson and A. Liebsch, Phys. Rev. B **28** (1983) 4247.

[27] J.C. Maxwell Garnett, Trans. of the Royal Society, (1904) v. CCIII 385.

[28] M. Ranjan, M. Bhatnager and S. Mukherjee, J. of Appl. Phys. **11** (2015) 103106.

[29] A. Manjavacas, ACS Photonics **3** (2016) 1301.

[30] C.A. Morrison and R.P. Leavitt 1982 *Handbook of the Physics and Chemistry of Rare Earths* vol. 5, ed. K.A. Geschneider and L. Eying (New York: North Holland) ch. 46, p. 461.

[31] S. Sturniolo and J.R. Yates, J. Chem. Phys. **150** (2019) 094103.

[32] R.D. Averitt, S. L. Westcott and N. J. Halas, J. Opt. Soc. Am. B **16** (1999) 1824.

[33] M.A. García, J. Phys. D.: Appl. Phys. **44** (2011) 283001.

[34] H.C. van de Hulst, *Scattering by Small Particles* Dover, New York 1981.

[35] Y. Chen, O. Höhn, N. Tucher, M.-E. Pistol and N. Anttu, Opt. Express **25** (2017) A665.

[36] V.A. Podolskiy and E.E. Narimanov, Phys. Rev. B **71** J. Phys. Chem. C **113** (2009) 7079.

[37] M.K. Kinnan, S. Kachan, C.K. Simmons and G. Chumanov, J. Phys. Chem. C **113** (2009) 7079.

[38] J.-Y. Chang, Y. Yang and L. Wang, Inter. J. of Heat and Mass Transfert **87** (2015), 237.

[39] M. Esslinger, R. Vogelgesang, N. Talebi, W. Khunsin, P. Gehring, S. de Zuani, B. Gompf and K. Kern, ACS Photonics **1** (2014) 1285.

[40] K. Dolgaleva, R.W Boyd and P.W. Milonni, J. Opt. A: Pure Appl. Opt. **11** (2009) 024002.

***Research Highlights**

Highlights:

-We report the optical response of a rectangular array of Ag NPs in uniaxial $LiNbO_3$.

-We investigate the anisotropic effects on the effective dielectric tensor taking into account the charges interaction of NPs.

-The effective dielectric tensor components of the ensemble are treated by an extended Maxwell-Garnett approximation.

-We show that the negative epsilon condition is satisfied for critical values of the structural parameters of the array.

-We show some anisotropic features on bandwidth and shift of resonance energies in the effective dielectric tensor components.

***conflict of Interest Statement**

Conflit of interest form:

We declare that we do not have any conflit of interest in the elaboration of this paper.

***Author Contributions Section**

Contribution of authors:

The manuscript was written through contributions of all authors. All authors have given approval to the final versión of the manuscript.